ELSEVIER

International Journal of Heat and Fluid Flow 20 (1999) 320–328

International Journal of
HEAT AND
FLUID FLOW

www.elsevier.com/locate/ijhff

Recent progress in the computation of flow and heat transfer in internal cooling passages of turbine blades

H. Iacovides *, M. Raisee

Department of Mechanical Engineering, UMIST, P.O. Box 88, Manchester M60 1QD, UK

Abstract

This paper describes our efforts to compute convective heat transfer through gas-turbine blade-cooling passages. The influence on the mean and turbulent flow due to surface rib-roughness is the main focus. A number of turbulence models, of effective viscosity (EVM) and second-moment type, are applied to the computation of flow and heat transfer through ribbed-roughened passages. Computations of flow through a rib-roughened U-bend show that second moment closures are necessary in order to correctly reproduce the regions of flow separation. Heat transfer computations through two-and also three-dimensional ribbed passages reveal that low-Re turbulence models are necessary and that a low-Re differential stress closure yields thermal predictions that are superior to those of the low-Re EVM model. A differential version of the Yap length-scale correction term, independent of the wall distance, is introduced to the dissipation rate equation and is found to improve the heat transfer predictions of the low-Re $k-\epsilon$ model.

1. Introduction

The design of effective internal cooling passages within the rotating blades of gas-turbines has been exercising the minds of engine designers for a number of decades. Flow in these passages is not only affected by the rotation of the blade, but also by the presence of sharp U-bends and heat-transfer-enhancing ribs. The resulting flow field is consequently complex and highly three-dimensional, containing regions of strong acceleration, flow separation and secondary motion. Wall heat transfer is highly non-uniform and even mean values cannot be accounted for by existing correlations. The development of numerical methods that can reliably predict wall heat transfer in such passages thus can greatly facilitate the design process.

Flow solvers used for the computation of such flows, need to be able to resolve the complex three-dimensional features of the mean motion with numerical accuracy and also to employ mathematical models of turbulence that reproduce the effects of separation, streamline curvature and rotation on the turbulence field. Moreover, since the main interest is in the computation of wall heat transfer, an additional and more challenging requirement is that the near-wall turbulence must also be faithfully reproduced. Progress in the development of suitable numerical techniques has been difficult, because of the heavy computational demands involved and also because of, until recently, the lack of detailed experimental data, against which turbulence models could be validated. This paper reports the authors' recent efforts to address some of the issues related to the computation of blade cooling flows, namely those of rib-roughness and strong curvature.

As far as the curvature effects are concerned, in flows through curved ducts, local imbalances between the curvature-induced centrifugal force and the opposing centripetal pressure gradient, lead to secondary motion, which transports fluid from the outer to the inner side of the curved duct. The fluid is then returned to the outer wall through the duct centre. As a result, the faster fluid is convected to the outer side of the curved passage. The secondary velocities are strongest at the near-wall regions. Thus in order to accurately predict the secondary motion, as shown by Choi et al. (1989) the near-wall regions and the viscous sub-layer regions would need to be adequately resolved. A subsequent study by Besserman and Tanrikut (1991) also showed that the resolution of the wall sub-layer, in place of the more widely used wall function approximation, improves heat-transfer predictions through curved ducts. In addition to the above effects on the mean motion, streamline curvature also has a direct effect on turbulence. As identified by Bradshaw (1973), the EVM approximation is unable to reproduce this effect. Consequently, as shown by numerous researchers, such as Iacovides and Li (1993), the non-symmetric velocity profiles that develop across curved channels (Ellis and Joubert, 1974), cannot be reproduced by EVM models. As far as three-dimensional flows through U-bends are concerned, Choi et al. (1989) and more recently Iacovides et al. (1996) have shown that flow predictions are improved through the introduction of second-moment closures. More elaborate realisable closures have been shown (Iacovides et al. (1996)) to be especially promising for the computation of heat transfer. In U-bends of strong curvature, which are common in blade-cooling passages, the measurements of Cheah et al. (1996), have revealed that the streamwise pressure gradients that develop at both ends of the bend exert the strongest influence. Within and downstream

* Corresponding author. E-mail: h.iacovides@unist.ac.uk.

0142-727X/99/$ – see front matter
PII: S0142-727X(99)00018-1

of the bend, there is a sizeable separation region along the inner wall and strong flow acceleration along the outer wall. The computations of Iacovides et al. (1995) suggest that the curvature-induced separation is more reliably reproduced by extending the use of second-moment closures across the viscous sub-layer.

Rib roughness, by causing flow separation, as can be seen in the data of Iacovides et al. (1995), leads to a substantial enhancement of turbulence levels. As can be seen in numerous experimental studies, Han (1984) and Iacovides et al. (1998b), heat transfer is also considerably enhanced. Moreover, the presence of ribs, as can be seen in the measurements of Humphrey and Whitelaw (1979), also induces or reinforces stress-gradient-difference secondary motion. The LDA study of Iacovides et al. (1998a), a follow-up study of the Cheah et al. (1996) investigation of a smooth U-bend, also examined the combined effects of rib-roughness and strong curvature, by introducing ribs of square cross-section along the inner and outer walls in the upstream and downstream sections, in a staggered arrangement. The study showed that the size of the curvature-induced separation bubble along the inner wall is reduced, while along the outer wall, when the accelerated fluid coming out of the bend encounters the first downstream rib, a large separation bubble is formed that covers the entire first rib interval. While some numerical studies of three-dimensional flows through ribbed passages have appeared, Taylor et al. (1991) and more recently Bonhoff et al. (1998), most have been confined to two-dimensional flows, like Liou et al. (1993). Finally the recent work of Rigby et al. (1996), also deserves a mention. Their multi-block approach highlights the need for adequate resolution of the corner regions, while the use of the Wilcox (1994) $k-\omega$ model returned reasonable Nusselt number distributions in smooth square-ended U-bend of strong curvature.

The first attempt within the authors' group to predict flow and heat transfer in three-dimensional ribbed passages, (Iacovides, 1998), involved the use body-fitted grids, which were shown to be numerically efficient. Zonal models of turbulence were employed, in which, either within an effective-viscosity approach, or a differential stress-closure, the dissipation rate of turbulence in the near-wall regions was obtained from the wall distance. This modelling approach was adopted because it allows the resolution of the sub-layer regions but without the need for very fine grid resolutions associated with low-Reynolds-numbers models, where the dissipation rate equation is integrated up to the wall. The mean flow and, when using a second-moment closure, the turbulence fields in straight ribbed passages were well predicted under both stationary and rotating conditions. The heat-transfer coefficient, however, was somewhat under-estimated. Here the zonal models are also used for flow computations in a ribbed U-bend, while as far as heat transfer computations are concerned, both zonal and low-Re models are tested for two- and three-dimensional straight ribbed passages. The U-bend flow computations have been carried out in order to test whether the zonal models can reproduce the combined effects of rib-roughness and strong curvature as well as those of rib-roughness and rotation (Iacovides, 1998). The heat transfer computations have been undertaken in order to explore whether the introduction of low-Re models correct the predictive deficiencies of the zonal models.

2. Flow equations

All the equations are presented in Cartesian tensor notation.

2.1. Mean flow equations

Continuity:

$$\frac{\partial}{\partial x_i}(\rho U_i) - 0. \tag{1}$$

Momentum transport:

$$\frac{\partial}{\partial x_j}(\rho U_i U_j) = -\frac{\partial P}{\partial x_i} + \frac{\partial}{\partial x_j}\left[\mu\left(\frac{\partial U_i}{\partial x_j} + \frac{\partial U_j}{\partial x_i}\right) - \rho\overline{u_i u_j}\right]. \tag{2}$$

Enthalpy:

$$\frac{\partial}{\partial x_j}(\rho U_i T) = \frac{\partial}{\partial x_j}\left[\frac{\mu}{\mathrm{Pr}}\frac{\partial T}{\partial x_j} - \rho\overline{u_j t}\right]. \tag{3}$$

2.2. Turbulence modelling equations

2.2.1. Effective-viscosity models

Stress–strain relationship:

$$\rho\overline{u_i u_j} = \frac{2}{3}k\delta_{ij} - \mu_t\left(\frac{\partial U_i}{\partial x_j} + \frac{\partial U_j}{\partial x_i}\right), \quad \mu_t = \rho c_\mu \frac{k^2}{\epsilon}.$$

Zonal $k-\epsilon$ model: This consists of the high-Re $k-\epsilon$ in the fully turbulent core:

$$\frac{\partial}{\partial x_j}(\rho U_j k) = \frac{\partial}{\partial x_j}\left[\left(\mu + \frac{\mu_t}{\sigma_k}\right)\frac{\partial k}{\partial x_j}\right] + P_k - \rho\epsilon, \tag{4}$$

$$P_k = -\rho\overline{u_i u_j}\left(\frac{\partial U_i}{\partial x_j}\right), \tag{5}$$

$$\frac{\partial}{\partial x_j}(\rho U_j \epsilon) = \frac{\partial}{\partial x_j}\left[\left(\mu + \frac{\mu_t}{\sigma_\epsilon}\right)\frac{\partial \epsilon}{\partial x_j}\right] + c_{\epsilon 1}\frac{\epsilon}{k}P_k - \rho c_{\epsilon 2}\frac{\epsilon^2}{k}. \tag{6}$$

In the near-wall regions, the high-Re $k-\epsilon$ is matched to Wolfshtein, 1969-equation model.

The k-transport equation is the same as Eq. (4) for the high-Re $k-\epsilon$. The dissipation rate, ϵ, and the turbulent viscosity, μ_t, are obtained from:

$$\epsilon = \frac{k^{3/2}}{l_\epsilon} \text{ and } \quad \mu_t = \rho c_\mu l_\mu \sqrt{k}. \tag{7}$$

The length scales l_ϵ and l_μ are obtained from the near-wall distance Y, according to:

$$l_\epsilon = 2.55Y[1 - \exp(-0.263y^*)], \tag{8}$$

$$l_\mu = 2.55Y[1 - \exp(-0.016y^*)]. \tag{9}$$

Launder–Sharma (Launder and Sharma, 1974) *low*-Re $k-\epsilon$:

$$\frac{\partial}{\partial x_j}(\rho U_j k) = \frac{\partial}{\partial x_j}\left[(\mu + \mu_t)\frac{\partial k}{\partial x_j}\right] + P_k - \rho\epsilon - 2\rho\nu\left(\frac{\partial\sqrt{k}}{\partial x_j}\right)^2, \tag{10}$$

$$\frac{\partial}{\partial x_j}(\rho U_j \epsilon) = \frac{\partial}{\partial x_j}\left[(\mu + \mu_t)\frac{\partial \epsilon}{\partial x_j}\right] + c_{\epsilon 1}\frac{\epsilon}{k}P_k - \rho c_{\epsilon 2} f_2 \frac{\epsilon^2}{k} + 2\rho\nu\nu_t\left[\frac{\partial^2 U_i}{\partial x_j \partial x_q}\right]^2, \tag{11}$$

where:

$$\mu_t = \rho c_\mu f_\mu k^2/\epsilon,$$

$$f_2 = 1 - 0.3\,\exp(-R_t^2), \quad f_\mu = \exp[-3.4/(1 + 0.02R_t)^2],$$

$$R_t = k^2/(\nu\epsilon). \tag{12}$$

2.2.2. Second-moment closures

The two variants employed here are relatively simple low-Re extensions of the basic differential stress closure. These extensions were first used by Iacovides and Toumpanakis, 1993.

Stress transport equations:

$$\frac{\partial}{\partial x_k}\left(\rho U_k \overline{u_i u_j}\right) = \frac{\partial}{\partial x_k}\left[\left(\mu + \frac{\mu_t}{\sigma_k}\right)\frac{\partial \overline{u_i u_j}}{\partial x_k}\right] + P_{ij} - \rho\epsilon_{ij} + \Phi_{ij} - \left[H_{ij} - \frac{1}{3}H_{kk}\delta_{ij}\right] + J_{ij}, \tag{13}$$

with P_{ij} and ϵ_{ij} obtained from:

$$P_{ij} = -\left[\overline{u_i u_k}\frac{\partial U_j}{\partial x_k} + \overline{u_j u_k}\frac{\partial U_i}{\partial x_k}\right], \tag{14}$$

$$\epsilon_{ij} = \frac{2}{3}(1 - f_\epsilon)\epsilon\delta_{ij} + f_\epsilon\frac{\overline{u_i u_k}}{k}\epsilon. \tag{15}$$

The redistribution term Φ_{ij} consists of the linear return-to-isotropy terms and of the conventional wall reflection terms that rely on the wall distance x_n and the unit vector to the wall n:

$$\Phi_{ij} = \Phi_{ij1} + \Phi_{ij2} + f_w(\Phi^w_{ij1}\Phi^w_{ij2}), \tag{16}$$

$$\Phi_{ij1} = -c_1\frac{\epsilon}{k}\left(\overline{u_i u_j} - \frac{2}{3}k\delta_{ij}\right), \tag{17}$$

$$\Phi_{ij2} = -c_2\left(P_{ij} - \frac{2}{3}P_k\delta_{ij}\right), \tag{18}$$

$$\Phi^w_{ij1} = c^w_1\frac{\epsilon}{k}\left(\overline{u_k u_m}n_k n_m\delta_{ij} - \frac{3}{2}\overline{u_k u_i}n_k n_j - \frac{3}{2}\overline{u_k u_j}n_k n_i\right)\left\{\frac{k^{1.5}}{\epsilon c_l x_n}\right\}, \tag{19}$$

$$\Phi^w_{ij2} = c^w_2\frac{\epsilon}{k}\left(\Phi_{km2}n_k n_m\delta_{ij} - \frac{3}{2}\Phi_{jk2}n_k n_j - \frac{3}{2}\Phi_{jk2}n_k n_i\right)\left\{\frac{k^{1.5}}{\epsilon c_l x_n}\right\}. \tag{20}$$

The low-Re terms H_{ij} and J_{ij} are defined as follows:

$$H_{ij} = f_H\frac{v}{k}\left(\overline{u_i u_l}\frac{\partial\sqrt{k}}{\partial x_l}\frac{\partial\sqrt{k}}{\partial x_j} + \overline{u_j u_l}\frac{\partial\sqrt{k}}{\partial x_l}\frac{\partial\sqrt{k}}{\partial x_i}\right), \tag{21}$$

$$J_{ij} = f_J k\left(\frac{\partial U_i}{\partial x_j} + \frac{\partial U_j}{\partial x_i}\right). \tag{22}$$

Zonal differential stress model (*DSM*):

The damping functions that appear in the above terms depend on the dimensionless wall distance $y^*/Yk^{1/2}/v$, have the following expressions:

$$f_\epsilon = \exp(-y^*/3),$$
$$f_w = [1 - \exp(-0.12y^*)][1 + \exp(-0.03y^*)],$$
$$f_J = 0.06\exp(-y^*/3),$$
$$f_H = (10.2 + 7.5y^*)\exp(-y^*/20).$$

In the fully turbulent region, the ϵ transport equation is the same as that of the high-Re k–ϵ model, Eq. (6).

In the near-wall regions, the dissipation rate, ϵ, is also obtained from a prescribed length scale l_ϵ, obtained from

$$l_\epsilon = 2.55Y[1 - \exp(-0.236y^*)].$$

Low-Re differential stress model (*DSM*): The damping functions now depend on the local Reynolds number of turbulence, $R_t \equiv k^2/v\epsilon$:

$$f_\epsilon = \exp(-R_t/8),$$
$$f_w = [1 - \exp(-R_t/20)][1 - \exp(-R_t/100)],$$
$$f_J = 0.06\exp(-R_t/8),$$
$$f_H = (10 + 2.6R_t)\exp(-R_t/20).$$

The dissipation rate equation used is the same as Eq. (11) for the low-Re Launder–Sharma k–ϵ. The damping function, f_μ, which still appears in the stress and ϵ transport equations is now obtained from:

$$f_\mu = \exp[-4/(1 + 0.01R_t)^2].$$

2.2.3. Length scale correction terms

It is well known, that in separated flows, the Launder–Sharma version of the ϵ equation returns excessively high levels of near-wall turbulence. To address this problem, Yap (1987) proposed the addition of a correction term to the ϵ equation, YC, based on the wall distance, Y.

$$\mathrm{YC} = \max\left|0.83\frac{\epsilon^2}{k}\left(\frac{k^{1.5}/\epsilon}{2.55Y} - 1\right)\left(\frac{k^{1.5}/\epsilon}{2.55Y}\right)^2, 0\right|. \tag{23}$$

In a recent proposal by Hanjalic (1996) the wall distance in the above term is eliminated by using the gradient of the length scale normal to the wall surface. Here, these ideas are further developed, by (a) introducing the resultant of the length scale gradient vector and (b) by also taking into account the effects of wall damping across the sub-layer.

From Woolfshtein: $l_\epsilon = 2.55\ Y[\,1 - \exp(-0.263\ y^*)\,]$.

Differentiating l_ϵ and then replacing y^* by R_t, as proposed by Yap (1987), produces the following expression for the gradient of the equilibrium length scale, $(\mathrm{d}l_e/\mathrm{d}Y)$:

$$(\mathrm{d}l_e/\mathrm{d}Y) = c_l[1 - \exp(-B_\epsilon R_t)] + B_\epsilon c_l R_t\ \exp(-B_\epsilon R_t)$$

with $c_l = 2.55$ and $B_\epsilon = 0.1069$.

From the resultant gradient, D_l, of turbulent length scale $l = k^{3/2}/\epsilon$, a correction factor F is defines according to:

$$D_l = (\mathrm{d}l/\mathrm{d}x_j)(\mathrm{d}l/\mathrm{d}x_j)^{1/2},$$
$$F = [(D_l - (\mathrm{d}l_e/\mathrm{d}Y)]/c_l.$$

A new version of the Yap term, NYC, is then developed:

$$\mathrm{NYC} = \max[0.83F(F+1)^2\rho\epsilon^2/k, 0.]. \tag{24}$$

2.3. Modelling of turbulent heat fluxes

In all EVM and some second-moment computations the turbulent heat fluxes have been modelled through the effective diffusivity approximation

$$\rho\overline{u_i t} = -\frac{\mu_t}{\sigma_T}\frac{\partial T}{\partial x_i}. \tag{25}$$

In most of the second-moment computations the generalised gradient diffusion hypothesis has been employed.

$$\overline{u_i t} = -\rho c_T\frac{k}{\epsilon}\overline{u_i u_j}\frac{\partial T}{\partial x_i}. \tag{26}$$

2.4. Modelling constants

The empirical constants that appear in the turbulence equations have the following values, according to the proposals of Jones and Launder (1972) for the k and ϵ equations and Gibson and Launder (1978) for the stress equations

c_μ	$c_{\epsilon1}$	$c_{\epsilon2}$	c_1	c_2	c^w_1	c^w_2	σ_k	σ_ϵ	σ_T
0.09	1.44	1.92	1.8	0.6	0.5	0.3	1	1.3	0.9

2.5. Numerical issues

The calculations presented here were carried out with a number of finite volume solvers. For two-dimensional computations a fixed, orthogonal co-ordinate solver has been used. Recent three-dimensional computation have been obtained using the STREAM code, which employs general non-orthogonal co-ordinates, with a Cartesian velocity decomposition. In the fully-elliptic, three-dimensional computations, a bounded version of the upstream quadratic interpolation scheme, QUICK, was employed for the discretization of convection in all transport equations, described elsewhere (Iacovides, 1997). Grid issues are discussed during the presentation of results.

3. Results and discussion

3.1. Flow computations

As mentioned in Section 1, one of the issues addressed in our earlier investigations (Iacovides, 1998; Iacovides, 1997) was that of achieving adequate grid resolution for three-dimensional flows through passages of complex geometries. It was shown that body-fitted grids allow the flow region around ribs to be resolved with fewer grid nodes than Cartesian grids with blocked regions and also prevent the formation of large-aspect-ratio cells within the flow domain. Body-fitted grids of relatively modest size were found to be able produce grid-independent solutions in ribbed passages.

Here we reproduce one of these earlier comparisons (Iacovides, 1997) for flow through a ribbed U-bend. The flow domain is shown in Fig. 1. Two body-fitted grids were used to resolve one of the symmetric halves of the flow domain shown in Fig. 1, a grid of $15 \times 32 \times 147$ shown in Fig. 2 and also a $21 \times 44 \times 297$ grid, both resulting in the same solutions. The measured (Iacovides et al., 1998a) flow development along the symmetry plane, presented in the velocity profiles of Fig. 3, is for the most part well predicted, especially when the zonal EVM is replaced by the zonal DSM closure. As also found in flows through smooth U-bends (Iacovides et al., 1995), the separation bubbles along both the inner and the outer walls are more faithfully reproduced by the zonal DSM, though, evidently, agreement with the experimental data is not complete. These findings are consistent with those of (Iacovides, 1998), regarding flow through straight ribbed passages, under stationary and rotating conditions.

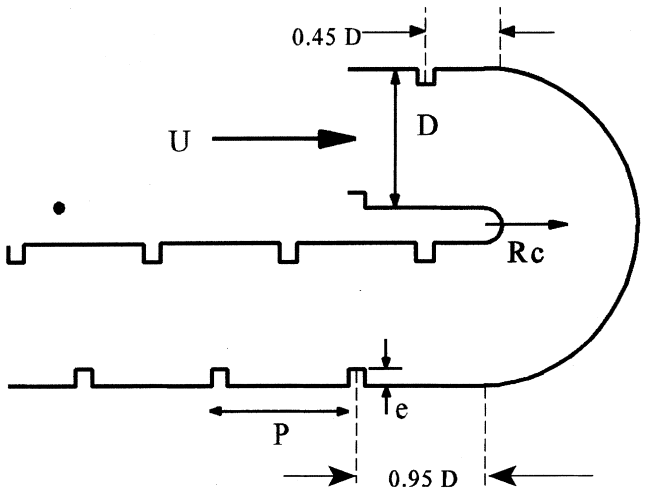

Fig. 1. Ribbed, rotating U-bend with staggered ribs.

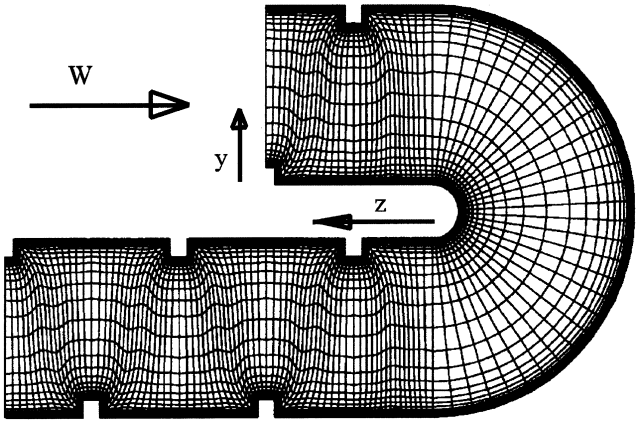

Fig. 2. Grid employed for computations through a ribbed U-bend.

3.2. Heat transfer in two-dimensional ribbed passages

Several flows through two-dimensional ribbed pipes and plane channels, such as those shown in Fig. 4, have been computed. Here, local Nusselt number comparisons are presented for two such cases, the details of which are tabulated below.

Passage	P/e	e/D or e/H	Re	Pr
Pipe	10	0.0675	64×10^3	0.71
Channel	10	0.1	40×10^3	5.45

All the cases examined, involved passages long enough for repeating flow conditions to prevail over each rib interval. Consequently, the numerical flow domain covers only one rib interval and repeating flow and thermal boundary conditions are applied. A Cartesian mesh is employed, with the grid nodes falling within the ribs blocked off. In all cases two grids were used, a 51×60 and a 91×110. For the first case constant wall heat flux thermal boundary conditions were employed. For the second case constant wall heat flux conditions were applied over the rib interval. The heat conduction equation was then solved within the ribs, assuming that the heat flux, per unit area, into each rib was the same as that for the rest of the duct wall. These thermal boundary conditions were consistent with the heating arrangements in the experimental study (Iacovides et al., 1998b).

The mean flow fields returned by the zonal EVM and DSM models for the ribbed pipe interval are shown in Fig. 5. Downstream of the rib, because of its sensitivity to streamline curvature, the DSM model predicts a longer and wider separation bubble. The corresponding low-Re models produced similar flow fields.

Comparisons for the local Nusselt number for the ribbed pipe, with the experimental data of Baughn and Roby, 1992 presented in Fig. 6, reveal that the two zonal models underpredict, by as much as 30%, Nusselt numbers over the first half of the rib interval, while over the second half of the interval, both models are in close agreement with the data. This is not unexpected, since in both zonal models, the scale of the near-wall eddies is assumed to depend on the wall distance, an assumption which is inappropriate for flow separation regions, where transport effects on the turbulent length scale cannot be ignored. In fact when the simplicity of the near-wall model is

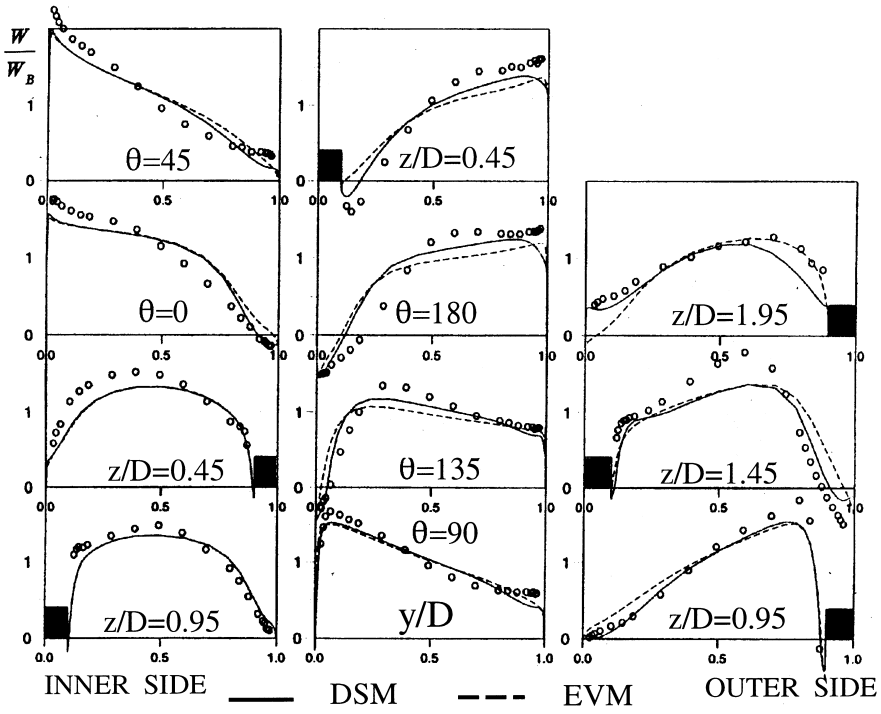

Fig. 3. Mean flow comparisons for flow along the symmetry plane of a ribbed U-bend.

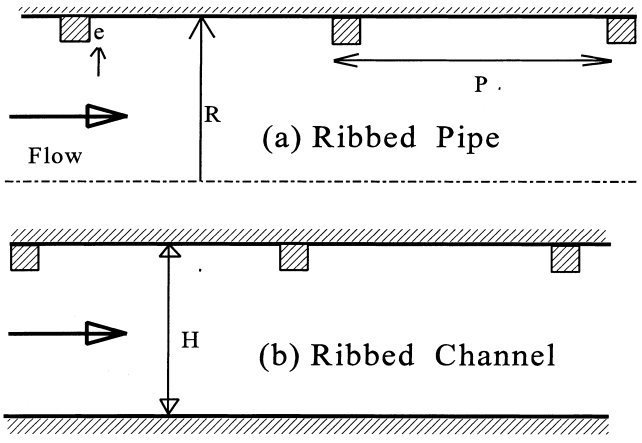

Fig. 4. Two-dimensional ribbed passages examined.

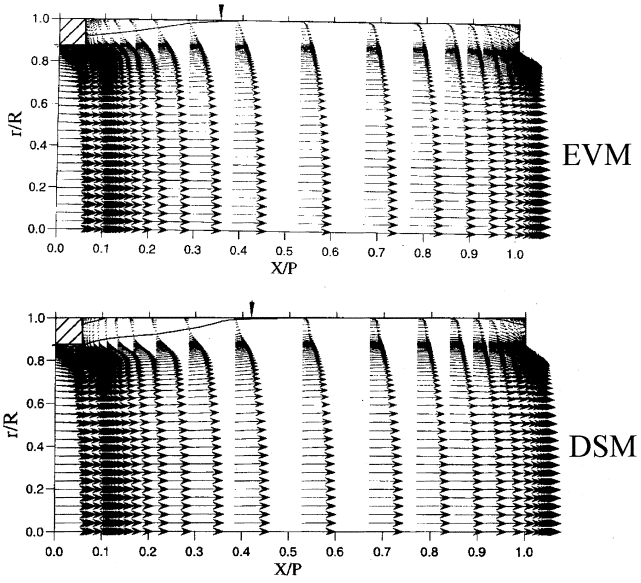

Fig. 5. Predicted mean flow field in a ribbed pipe.

taken into account, the thermal predictions of the zonal approaches can be said to be surprisingly close to the data. The zonal EVM predicts that downstream of the rib the Nusselt number rises too quickly to its local maximum, while the zonal DSM shows the opposite predictive deficiency. The low-Re $k-\epsilon$ with the old Yap term over- predicts levels of wall heat transfer, by about 20%, while with the new Yap term proposal, agreement with the measured Nusselt number data is very close. The low-Re DSM with the new Yap term returns too low Nusselt number values downstream of the interval, but with the old Yap term the predicted Nusselt number variation is in closer overall agreement with the data, over the rib interval and also over the rib surface.

Comparisons for the ribbed channel, with water as the working fluid, $Pr = 5.45$, shown in Fig. 7, also lead to similar conclusions. It should be noted, that the ribbed channel, was in fact of a square cross-section, but, as shown in (Iacovides et al., 1998b), the measured variation in the local Nusselt number in the lateral direction was minimal. The measurements also show that in the plane channel Nusselt number levels rise more gradually downstream of the rib, possibly because only one wall of the plane channel is ribbed and consequently each rib causes a stronger deflection of the flow away from the ribbed surface. The DSM models reproduce this gradual rise more faithfully than the EVM and are therefore in closer agreement with the thermal data.

The two-dimensional comparisons therefore, for axisymmetric and plane geometries, indicate that the zonal models under-predict wall heat transfer, but are in reasonable overall

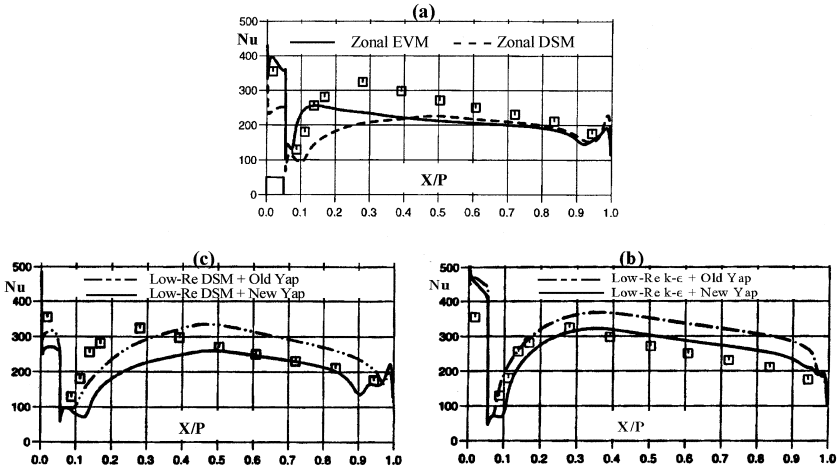

Fig. 6. Nusselt number comparisons for ribbed piped, at $Re = 64 \times 10^3$.

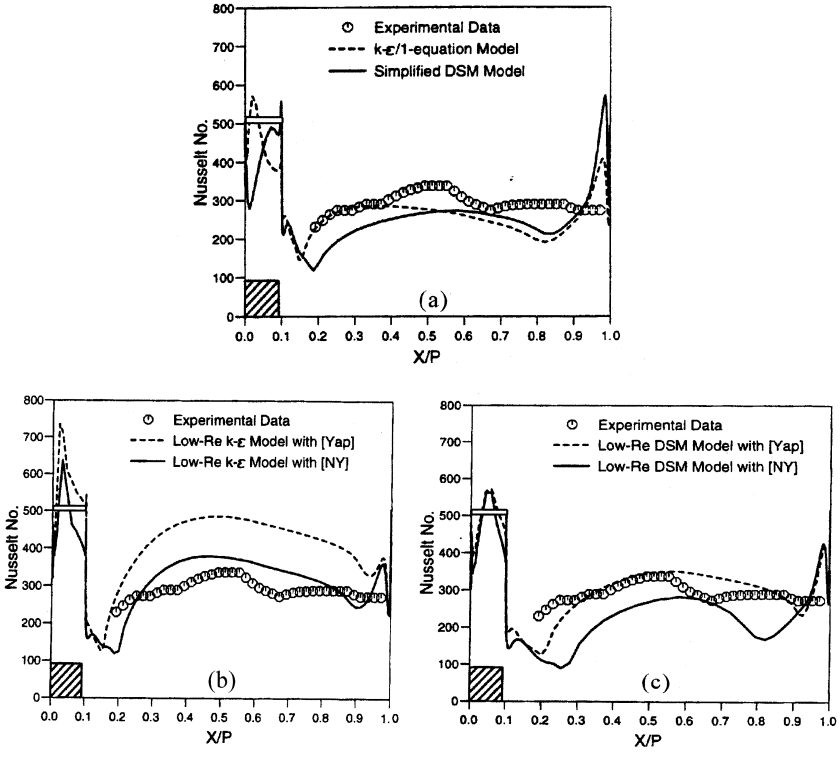

Fig. 7. Nusselt number comparisons for ribbed channel, at $Re = 40 \times 10^3$, and $Pr = 5.45$.

accord with measured heat transfer data. The new Yap term improves the thermal predictions of the low-Re EVM, resulting in good agreement with the data, while for the low-Re DSM the effect of the new Yap term appears to be too strong leading to unrealistically low levels of wall heat transfer. A re-optimisation of this term appears to be necessary when used with the low-Re DSM tested in this study. The recent work of Craft, 1998 in which this differential form of the Yap term has been included in another low-Re DSM model for the computation of impinging jet flows, also reached the same conclusion.

Mean flow comparisons, not shown here, show practically no difference between predictions obtained by the two different versions of the Yap term. The changes that the differential form of the Yap term causes to the heat transfer predictions arise from the effect that this term has on the turbulence across the viscous and transition layers.

3.3. Flow and heat transfer in three-dimensional ribbed passages

Heat transfer computations have straight ribbed ducts of square cross-section in which repeating flow conditions are established. Two such geometries, shown in Fig. 8, have been examined: a straight duct with in-line ribs on opposite walls, and a duct with staggered ribs on opposite walls. In the case of the duct with in-line ribs, the rib-height-to-diameter ratio, e/D is 0.0675, the rib spacing, P/e is 10 and data for comparison have been obtained from Baughn and Yan, 1992. For the duct with staggered ribs, $e/D = 0.1$ and $P/e = 10$, and the

case was experimentally examined at UMIST (Iacovides et al., 1998a).

The rib intervals were resolved using a $74 \times 62 \times 30$ body-fitted mesh. While there are fewer grid-nodes in the cross-stream direction than in the two-dimensional computations, where Cartesian grids were used, the body-fitted meshes employed in the three-dimensional computations, as can be seen in Fig. 2, allow a more efficient resolution of the near-wall regions. The y^+ value of the near-wall nodes was kept, in all computations, to levels less than 1.

Comparisons of the Nusselt number distribution along the symmetry line of the ribbed wall, for the duct with in-line ribs, Fig. 9, show that the zonal models, as in the two-dimensional cases, under-predict the coefficient of wall heat transfer. The zonal DSM does however reproduce the experimental behaviour more closely than the zonal EVM, returning a more gradual rise in Nusselt number in the recirculation region downstream of each rib and higher levels after re-attachment. The low-Re EVM returns higher Nusselt numbers which, especially with the new Yap term, are very close to the measured values. In common with the zonal EVM and also as noted in two-dimensional channels, the low-Re EVM predicts that in the recirculation region downstream of each rib, the Nusselt number rises too quickly. As also noted in the two-dimensional cases, with the original Yap term the low-Re $k-\epsilon$ over-predicts wall heat transfer. The low-Re DSM comparisons for this case, also lead to conclusions similar to those reached in the two-dimensional case. With the original Yap term, the low-Re DSM produces a Nusselt number distribution that for the most part is close to the measurements and also, in contrast to the EVM, returns a more gradual rise downstream of each rib.

For the passage with staggered ribs, comparisons are presented, for the distribution of local Nusselt number along the symmetry line of the ribbed wall and also for the distribution of the side-averaged Nusselt number along the ribbed wall, Fig. 10. The zonal model predictions, show that the Nusselt number is now more severely under-predicted than for the duct with in-line ribs. One possible cause may be the fact that the rib size in this case is greater. As expected, the introduction of low-Re models leads to the prediction of higher Nusselt numbers. The low-Re EVM, with the original Yap term, while, as in the previous cases, over-predicting the symmetry-line Nusselt number, nevertheless returns the correct distribution of the side-averaged Nusselt number. With the new version of the Yap term, the low-Re $k-\epsilon$ returns reasonable Nusselt number values along the symmetry line, but under-predicts the side-averaged Nusselt number. The low-Re DSM, with the original Yap term returns the correct distribution of wall heat transfer along the symmetry plane and also the correct distribution of the side-averaged Nusselt number.

The three-dimensional heat-transfer computations therefore result in conclusions that are on the whole consistent with those reached in the computations of two-dimensional flow and heat transfer through ribbed passages. Zonal models, because they ignore the effects of transport on the near-wall turbulence scale, under-predict wall heat transfer rates. The

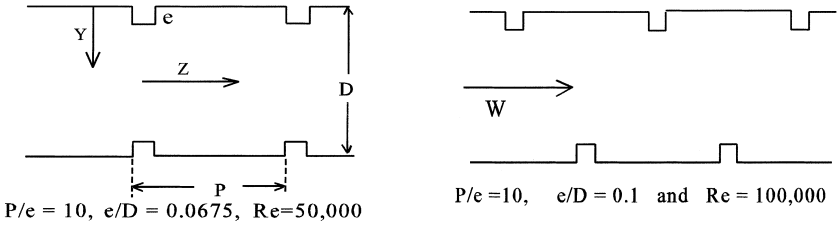

(a) Square duct with in-line ribs (b) Square duct with staggered ribs

Fig. 8. Flow geometries and conditions for ribbed ducts.

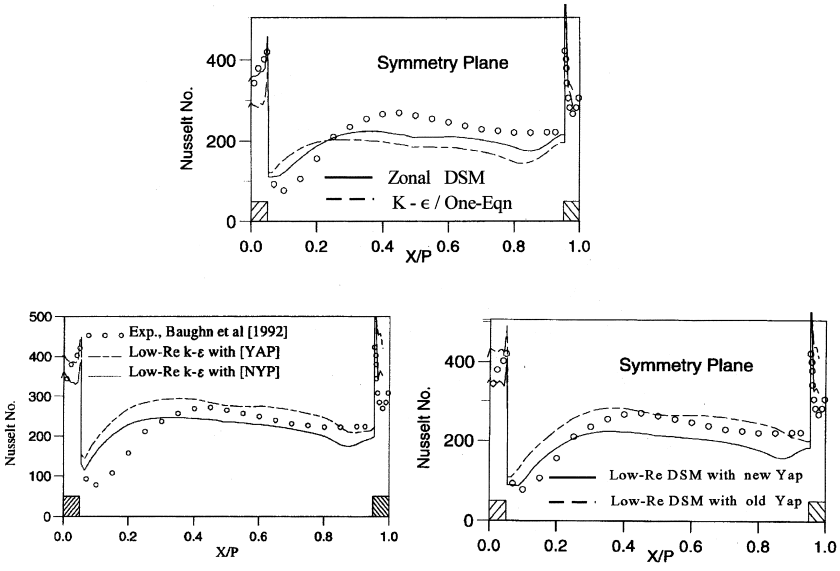

Fig. 9. Local Nusselt number comparisons, along the duct symmetry line, for repeating flow in a square duct with in-line ribs: $Re = 50{,}000$; $Pr = 0.71$.

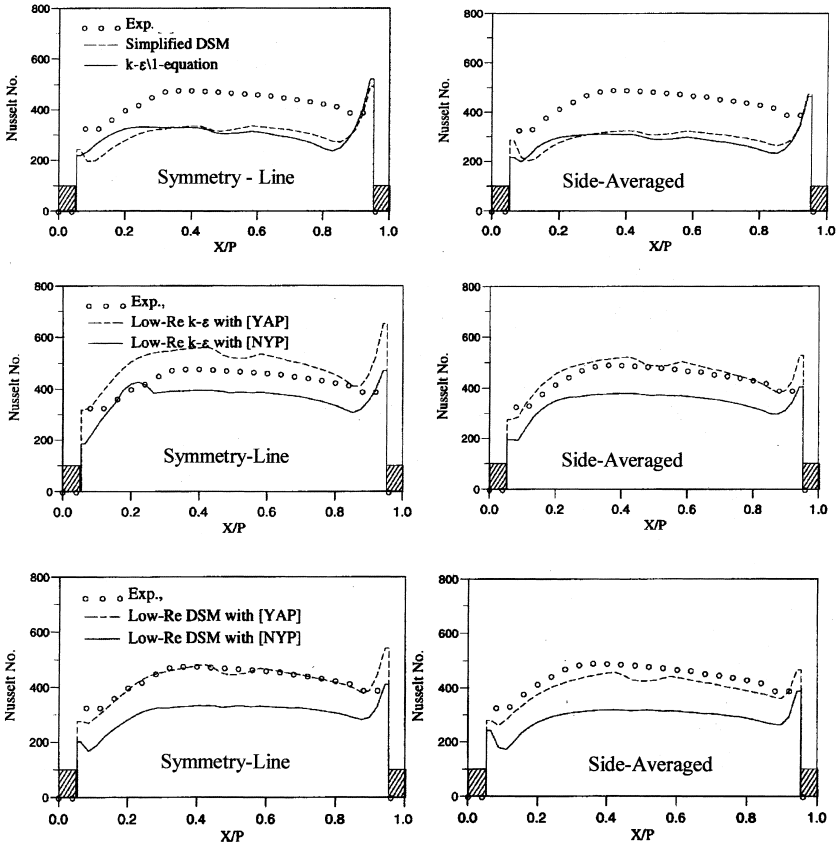

Fig. 10. Nusselt-number comparisons for repeating flow through a heated duct with staggered ribs: Re = 100,000 and Pr = 0.71.

low-Re closures are found able to reproduce the correct Nusselt numbers, provided that correction terms are added to the dissipation rate equation. The alternative version to the Yap term proposed, appears to offer some predictive advantages when used with the low-Re EVM model, but in its current form is found to be too strong when used with the low-Re DSM closure. The second-moment closure, low-Re extension of even the basic DSM model, is found to produce heat transfer predictions that are superior to those of the EVM model and in close accord with the available data.

4. Concluding remarks

The computation of flow and convective heat transfer in passages affected by strong curvature and rib-roughness has been considered. A series of test cases have been computed, in order to identify the turbulence modelling practices necessary to produce reliable predictions in flows subjected to these influences. For the computation of three-dimensional flows through ribbed passages of complex geometries, as shown in our earlier studies, the use of body-fitted grids has been found to substantially reduce grid requirements. For the computation of flows affected by strong curvature and rib-roughness it is found necessary to extend the second-moment closure across the viscous sub-layer. As far as the computation of heat transfer through ribbed passages is concerned, the use of low-Re closure appears to be essential. For the low-Re closures tested the inclusion of length scale correction term appears to be necessary. For the low-Re $k-\epsilon$ an alternative to the Yap term, independent of the wall distance, is found to be more promising than the original version. The low-Re DSM model, because of its sensitivity to the effects of streamline curvature reproduces the turbulence field more faithfully than the EVM model, which in turn leads to thermal predictions superior to those of the low-Re $k-\epsilon$. While agreement with measurements has not been complete in all the cases examined and further work on more complex flows is still in progress, low-Re differential stress models appear to offer the most promising route for the reliable computation of convective heat transfer in blade cooling passages.

Acknowledgements

Funding for the work presented has been provided by Rolls-Royce plc. The authors gratefully acknowledge both the financial and technical support received and the many useful interactions with Mr J. Coupland from Rolls-Royce Derby. The authors also wish to acknowledge the support and encouragement received from Prof. B.E. Launder. The help of Dr. Y.-M. Yuan and Mr G. Kelemenis who made their experimental data available in digital form, is also acknowledged.

References

Baughn, J.W., Yan, X., 1992. Local heat transfer measurements in square ducts with transverse ribs. ASME, National Heat Transfer Conference.

Baughn, J.W., Roby, J., 1992. HTD-Vol 202, ASME 28th National Heat Transfer Conference. San Diego, California.

Besserman, D.L., Tanrikut, S., 1991. Comparison of heat transfer measurements with computations for turbulent flow around a 180°

bend. ASME Paper 91-GT-2, Int. Gas-Turbine and Aero Congress, Orlando, FL.

Bonhoff, B., Parneix, S., Leusch, S., Johnson, B.V., Schabacker, J., Bolcs, A., 1998. A experimental and numerical study of development flow and heat transfer in coolant channels with 45° and 90° ribs. Proceedings of Second EF Conference on Turbulent Heat Transfer, Manchester, UK, pp. 7.29–7.41.

Bradshaw, P., 1973. Effects of streamline curvature on turbulent flow. AGARDograph 169.

Cheah, S.C., Iacovides, H., Jackson, D.C., Ji, H., Launder, B.E., 1996. LDA investigation of the flow development through rotating U-ducts. ASME J. Turbomachinery 118, 590–596.

Choi, Y.D., Iacovides, H., Launder, B.E., 1989. A numerical computation of turbulent flow in a square-sectioned 180° bend. ASME J. Fluids Eng. 111, 59–68.

Craft, C.J., 1998. A prediction of heat transfer in turbulent stagnation flow with a new second-moment closure. Proceedings of Second EF Conference on Turbulent Heat Transfer, Manchester, UK, pp. 4.15–4.25.

Ellis, L.B., Joubert, P.N., 1974. A turbulent shear flow in a curved channel. J. Fluid Mechanics 62, 65–84.

Gibson, M.M., Launder, B.E., 1978. A ground effects on pressure fluid fluctuations in atmospheric boundary layers. J. Fluid Mechanics 86, 491.

Han, J.C., 1984. A heat transfer and friction characteristics in channels with two opposite rib-roughened walls. ASME J. Heat Transfer 106, 774–781.

Hanjalic, K., 1996. Some resolved and unresolved issues in modelling non-equilibrium and unsteady turbulent flows. Proceedings of Third International Symposium on Engineering Turbulence Modelling and Measurements, Crete, Greece.

Humphrey, J.A.C., Whitelaw, J.H., A turbulent flow in ducts with roughness. Proceedings of Second International Symposium on Turbulent Shear Flow, London.

Iacovides, H., Li, H.Y., 1993. Near-wall turbulence modelling of developing flow through curved ducts and channels. Proceedings of IAHR, Fifth International Symposium on Refined Flow Modelling and Turbulence Measurements, Paris.

Iacovides, H., Toumpanakis, P., 1993. A turbulence modelling of flow in axisymmetric rotor-stator systems. Proceedings of IAHR, Fifth International Symposium on Refined Flow Modelling and Turbulence Measurements, Paris.

Iacovides, H., Launder, B.E., Li, H.Y., 1995. The computation of flow development through stationary and rotating U-bends of strong curvature. Int J. Heat and Fluid Flow 17, 22–23.

Iacovides, H., Launder, B.E., Li, H.Y., 1996. A application of a reflection-free DSM to turbulent flow and heat transfer in a square-Sectioned U-Bend. Int. J. Exp. Thermal and Fluid Science 13, 419–429.

Iacovides, H., 1997. The computation of turbulent flow through stationary and rotating U-bends of with rib-roughened surfaces. Proceedings of 11th International Conference on Lam and Turb. Flows, Swansea.

Iacovides, H., Jackson, D.C., Ji, H., Kelemenis, G., Launder, B.E., Nikas, K., 1998a. LDA study of flow development through an orthogonally rotating U-Bend of strong curvature and rib-roughened walls. ASME J. Turbomachinery 108, 386–391.

Iacovides, H., Jackson, D.C., Kelemenis, K., Launder, B.E., Yuan Y.M., 1998. A Recent progress in the experimental investigation of flow and local wall heat transfer in internal cooling passages of gas-turbine blades. Second EF Conference on Turbulent Heat Transfer, Manchester, UK, pp. 7.42–7.57.

Iacovides. H., 1998. A computation of flow and heat transfer through rotating ribbed passages. Int. J. Heat and Fluid Flow 19, 393–400.

Jones, W., Launder, B.E., 1972. A the prediction of laminarization with a two-equation model of turbulence. Int. J. Heat Mass Transfer 15, 301–314.

Launder, B.E., Sharma, B.I., 1974. Application of the energy-dissipation model of turbulence to the calculation of flow near a spinning disc. Letrs in Heat Mass Trans. 1, 131–138.

Liou, T.M., Hwang, J.J., Chen, S.H., 1993. A simulation and measurement of enhanced turbulent heat transfer, in a channel with periodic ribs on one principal wall. Int. J. Heat and Mass Transfer 36, 507–517.

Rigby, D.L., Ameri, A.A., Steinhorsson, E., 1996. A Internal passage heat transfer prediction using multi block grids and $k-\omega$ a turbulence model. ASME Paper, 96-GT-188.

Taylor, C., Xia, J.Y., Medwell, J.O., Morris, W.D., 1991. A Numerical simulation of three-dimensional turbulent flow and heat transfer within a multi-rib cylindrical duct. ASME, Paper 89-GT-8, International Gas-Turbine and Aero Congress.

Wilcox, D.C., 1994. A simulation of transition with a two-equation turbulence model. AIAA J. 23 (2), 247–255.

Wolfshtein, M., 1969. The velocity and temperature distribution in one-dimensional flow with turbulence augmentation and pressure gradient. Int. J. Heat and Mass Transfer 12, 301.

Yap, C.R., 1987. Turbulent heat and momentum transfer in recirculating and impinging flows. Ph. D. Thesis, Department of Mechanical Engineering, Faculty of Technology, University of Manchester.